Solid Freeform Fabrication 2019: Proceedings of the 30th Annual International
Solid Freeform Fabrication Symposium – An Additive Manufacturing Conference
Reviewed Paper

PERMEABILITY ANALYSIS OF POLYMERIC POROUS MEDIA OBTAINED BY MATERIAL EXTRUSION ADDITIVE MANUFACTURING

M. O. Shigueoka[*], S. L. de M. Junqueira[†], T. A. Alves[‡] and N. Volpato[*]

[*]Additive Manufacturing and Tooling Group (NUFER), Federal University of Technology - Paraná (UTFPR), Curitiba - PR, CEP: 81280-340
[†]Research Center for Rheology and Non-Newtonian Fluids (CERNN), Federal University of Technology - Paraná (UTFPR), Curitiba - PR, CEP: 81280-340
[‡]Laboratory of Porous Media and Energy Efficiency (LabPMEE), Federal University of Technology - Paraná (UTFPR), Ponta Grossa – PR, CEP 84016-210

Abstract

Porous media (PM) are used in many applications, and their geometry and hydraulic properties are essential in flow analysis, especially in geology (oil and gas) and medical (tissue engineering) applications. Additive Manufacturing (AM) enables the production of planned porosity and the material extrusion AM allows working with process parameters to produce lattice type geometries, without the need to have a 3D model of the internal porous structure. This work presents a preliminary study on the permeability of some PM designs obtained in PLA using an in-house process-planning software. Two main filling variations of the raster strategies were studied, one considering the displacement of staggered layers and the other involving a new joined filaments proposal. The permeability obtained experimentally is compared with numerical outputs. The results indicate that both filling strategies influence the PM permeability, but this was more significant with the joined filaments approach.

Keywords: Porous media, Permeability, Material extrusion

Introduction

Porous materials or porous media (PM) are found in applications related to power generation, vibration suppression, thermal insulation, sound absorption, fluid filtration, and others. One of their main mechanical characteristics is to present structural rigidity with low mass density [1]. When the objective is the fluid-flow analysis inside the PM, its geometry and properties, such as permeability and porosity, are of great interest, especially to areas such as geology, for application in the oil and gas industry, and medical applications, for tissue engineering [2], [3].

The relevance of Additive Manufacturing (AM) or 3D Printing in PM manufacturing is increasing, as it enables the production of planned porosity [4] and allows creating many replicas of the same PM, contributing to the statistical analysis of the experimental results. This is a relevant issue among others in geology because of the difficulties to have many specimens to test [3]. The material extrusion AM processes offer an important differentiation in this area because they allow working with process parameters to produce lattice-type geometries, without the need to 3D-model each filament (strut) of the internal porous structure in a CAD system [5]. The material deposited in a filament shape in the X-Y plane (layer addition plane) can create “lattice strut” in fiber-shaped structures, which can generate a porous matrix with a controlled design of the geometry, size, and arrangement of the pores.

A typical path filling in this AM technology is the raster strategy, also known as rectilinear filling, which is a zigzag path, formed with parallel lines. Here, by choosing a positive road gap

and a variation in the raster angle between successive layers, different pores geometries are generated [5]–[11]. One variation of this alternative is the possibility to apply a staggered raster, which consists of generating a lateral displacement of the raster fill pattern between the layers with the same raster angle, maintaining the road gap initially defined [9–11].

This work presents a preliminary study on the permeability of PM obtained by this AM principle. Some PM designs were printed in poly(lactic acid) (PLA) with two main filling strategies, one varying the stagger distance between layers and a new proposal not explored so far, which is a strategy involving joining filaments, both based on the raster strategies. The permeability was measured experimentally and obtained via numerical analysis.

Porous media by material extrusion AM

Instead of designing the PM in a CAD (Computer-Aided Design) system, the internal structure was obtained directly by controlling the process parameters of the material extrusion AM technology. The raster filling was selected as it is suitable to produce lattice type geometries that are scaffold structure of fibers alike. Fig. 1a and 1b show schematically the conventional distribution of a basic lattice PM, created by the combination of parameters like raster angle, its rotation, and the road gap. The staggered raster concept is shown in Fig. 1c, which consists of displacing laterally the raster filaments (raster lines) in relation to the previous layer with the same raster angle, maintaining the road gap defined. The main hypothesis behind this idea is that by increasing the tortuosity of the PM (i.e., the ratio between the distance travelled by the fluid and the characteristic length of the PM), its permeability is reduced. For this study, three stagger distances were used (0%, 25%, and 50%) as a percentage of the hatch distance between the filaments.

Joined filaments is a new raster strategy where two or more filaments (also referred to as raster lines) are printed side-by-side (zero gap) forming a set of filaments, and a gap is left between successive sets (see Fig. 1d). This pattern is repeated forming the path filling. A zero or negative Road Gap can be used inside the sets of filaments to ensure that there are no holes along with the contact areas. A new raster parameter was created namely Set Gap, which defines the distance between the set of joined filaments (lines sets, see Fig. 1d). In this work, single (i.e., no joined filaments) and sets of two joined filaments were selected for the analysis.

A relevant parameter to produce a PM in this technology is the minimum road gap or set gap (when considering joined filaments) that would guarantee that two adjacent filaments that have to create a pore (or a pore throat) would not touch each other. This is important to allow pores connectivity. Considering the precision and resolution of the 3D printer used in this work (3D Cloner DH+), the minimal road gap was identified as 0.1 mm. Thus, the theoretical porosity value obtained considering a filament cross section as an ellipse (d_1 /d_2=0.3 mm/0.44 mm, see Fig. 1b), was 35.9%. This porosity was fixed for all planned geometries presented below. As the road width and layer thickness are the same for all geometries, the set gap was responsible for maintaining the constant porosity, therefore it was varied accordingly.

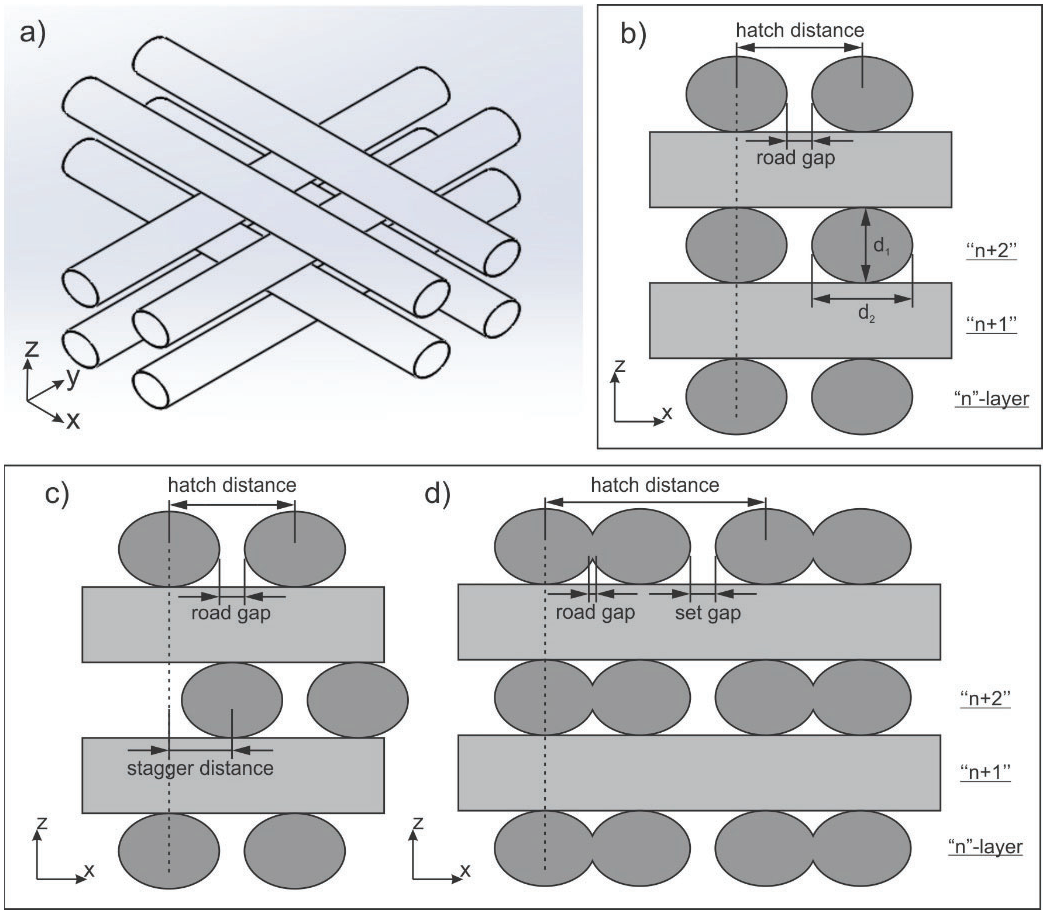

Fig. 1 - Schematic of raster parameters (a), filament cross section (b), stagger distance (c) and the new joined filaments raster strategy (d)

The parameters stagger distance (0%, 25%, and 50%) and number of filaments (lines) in a set (1 and 2) were combined creating six different PM designs, which were called L01S00 (meaning 1 filament and stagger distance 0), L01S25, L01S50, L02S00, L02S25, and L02S50 (Table 1).

The PM specimens had a cylindrical shape (diameter 25.4 mm and length 24 mm) to fit in the experimental apparatus core holder (Fig. 2a and b). For each configuration, five samples were produced, resulting in 30 specimens. The following parameters and conditions were used to manufacture the specimens: layer thickness 0.3mm; print speed 25 mm/s, extruder temperature 205 °C, bed temperature 50 °C, room temperature 26 °C, and relative humidity 65%.

As the process planning software currently available still have limitations on the level of customization of the path filling, an in-house process-planning software called RP3 (Rapid Prototyping Process Planning) was used to generate all manufacturing data (G-code)[12]. To check the final printed PM geometry, one of the PM design was digitally reconstructed by X-ray micro tomography (Carl Zeiss' Metrotom 1500).

Table 1 – Selected raster parameters for the designed PM

	Raster Parameters	
Designed PM	Lines in set (Joined filaments)	Stagger distance (Staggered)
L01S00	1	0%
L01S25	1	25%
L01S50	1	50%
L02S00	2	0%
L02S25	2	25%
L02S50	2	50%

Permeability Characterization

The permeability characterization was carried out using the direct experimental method, measuring the pressure drop that the fluid flow undergoes when permeating the PM sample, with the flow occurring in the axial direction (Fig. 2b). For the measurement, a permeameter (Fig. 2a) based on MPIF Standard 39 [13] was used with airflow at room temperature of 25 °C and a digital manometer (Digitron P200HIS) on the outlet. The volumetric flow rate varied from 6 to 30 l/min, with increments of 4 l/min, controlled by a rotameter, and with an inlet pressure of 3.5 bar. The permeability was calculated using the Dupuit-Forchheimer equations, obtaining the k_1 and k_2 Darcian and non-Darcian permeability constants [14].

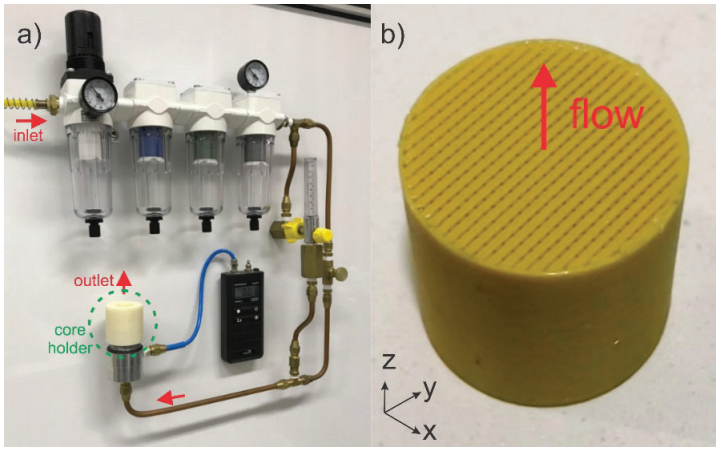

Fig. 2 – Experimental permeameter (a) and the printed PM showing the fluid flow direction (b)

Numerical simulations were conducted in the Fluid Simulation module of Solidworks 2018 with a modeled wind tunnel (Fig. 3) and using the same airflow conditions as in the experimental measurements. To speed up the numerical simulation, the size of the PM was reduced to a diameter of 6 mm with a length of 3.6 mm, but maintaining the same layer thickness and road gap of the experimental specimens. All PM 3D designs were modeled in the Open SCAD [15].

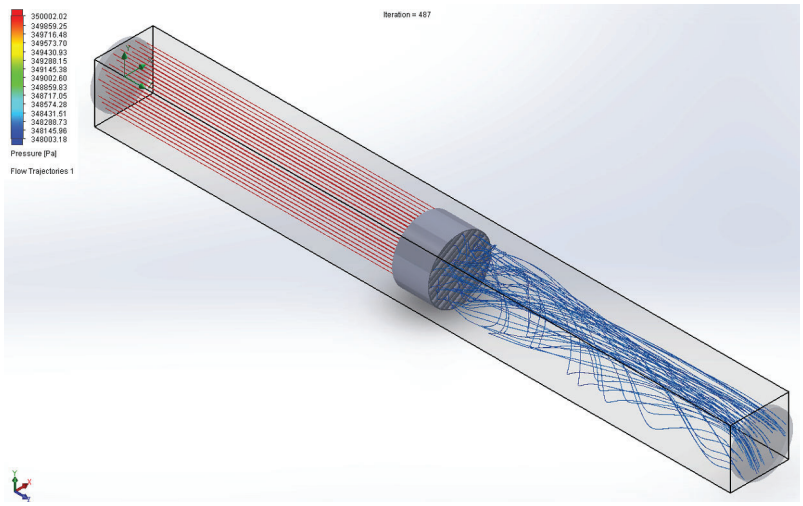

Fig. 3 –Wind tunnel in which the 3D models of the PM were simulated in Solidworks

Results and Discussions

All specimens were manufactured as planned (designed) by the RP3. This can be observed in the cross sections of the L02S50 (Fig. 4) obtained by cutting the 3D geometric model that was digitally reconstructed from the X-ray micro tomography.

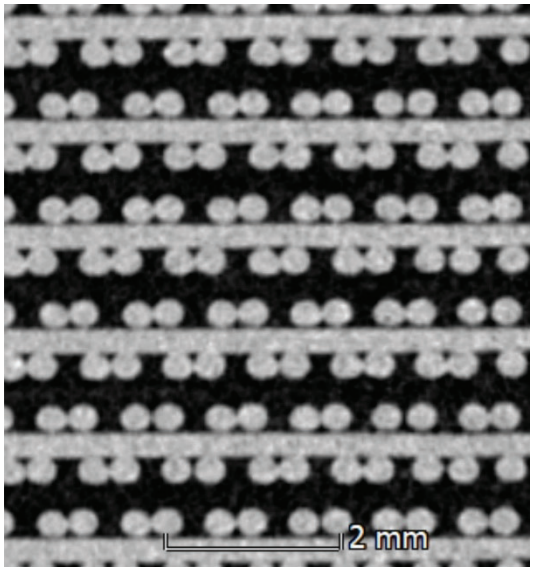

Fig.4 - Cross section of the L02S50

Graphs of the normalized pressure drop (the pressure drop results were divided by the specimens' lengths) in terms of the velocity impinged to the experimental and the numerical samples, for geometries with a set of 1 or 2 filaments (lines), are displayed in Fig. 5 and Fig. 6, respectively. The Darcian permeability values calculated using the Dupuit-Forchheimer equation are displayed in Table 2. Graphs for a comparison of the Darcian permeability values obtained from numerical simulation and experimental measurement are shown in Fig. 7.

Table 2 - Darcian permeability values calculated using the Dupuit-Forchheimer equation

	Darcian Permeability k_1 [10^{-9} m^2]		Non-Darcian Permeability k_2 [10^{-3} m]		Squared Correlation Coefficient R^2	
Designed PM	Exp.	Num.	Exp.	Num.	Exp.	Num.
L01S00	2.773	3.441	2.117	5.686	0.999975	0.999944
L01S25	2.610	3.461	2.076	4.474	0.999968	0.999676
L01S50	2.319	3.445	2.121	4.301	0.999963	0.999936
L02S00	7.274	7.680	1.291	2.201	0.999996	0.999324
L02S25	2.245	3.305	1.040	1.107	0.999983	0.998239
L02S50	1.718	2.651	0.754	0.784	0.999984	0.999182

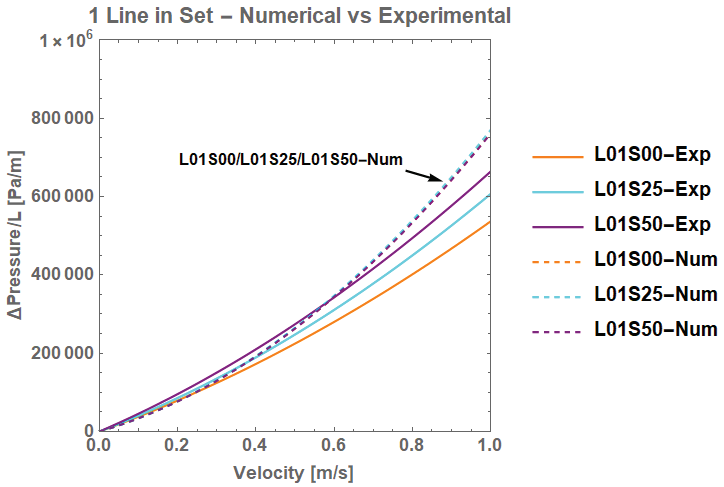

Fig. 5 – Graph Velocity vs. Normalized Pressure drop for the experimental measurement and the numerical simulation of PM with 1 line in set

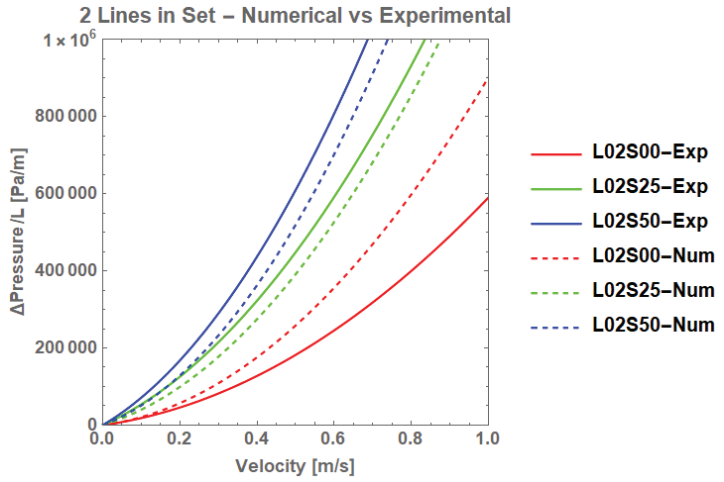

Fig. 6 – Graph Velocity vs. Normalized Pressure drop for the experimental measurement and the numerical simulation of PM with 2 lines in set

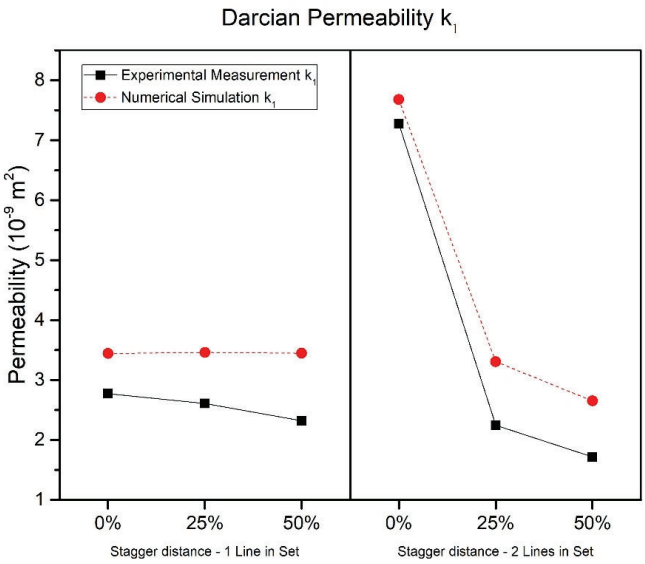

Fig. 7 - Darcian permeabilities k_1 versus the stagger distance for both line sets configuration.

In the configurations with 1 filament in the set (L01S00, L01S25, and L01S50), the pressure drop curves presented little variation for both the experimental and numerical simulations (Fig. 5). The statistics "student's t-tests" combining the 3 simulation results (with a confidence level of 99.5%) do not reject the probability that the values represent the same behavior of the interaction Velocity vs. Pressure drop. Although the numerical results for staggering shown in Fig. 7 (set of 1 filament) indicates a quite similar permeability as the stagger distance increases, the experimental measurements demonstrated a decrease in permeability.

In Fig. 6 and Fig. 7, one observes that for the PM with 2 joined filaments (lines) in the set (L02S00, L02S25, and L02S50), both experimental and numerical results pointed to the same tendency of decreasing in permeability with the increase of the stagger distance. Fig. 8 shows the contrasting streamlines paths in L02S00 and L02S50, which help to explain the change in tortuosity of the PM when increasing the stagger distance, and, consequently, the fluid flow restrictions.

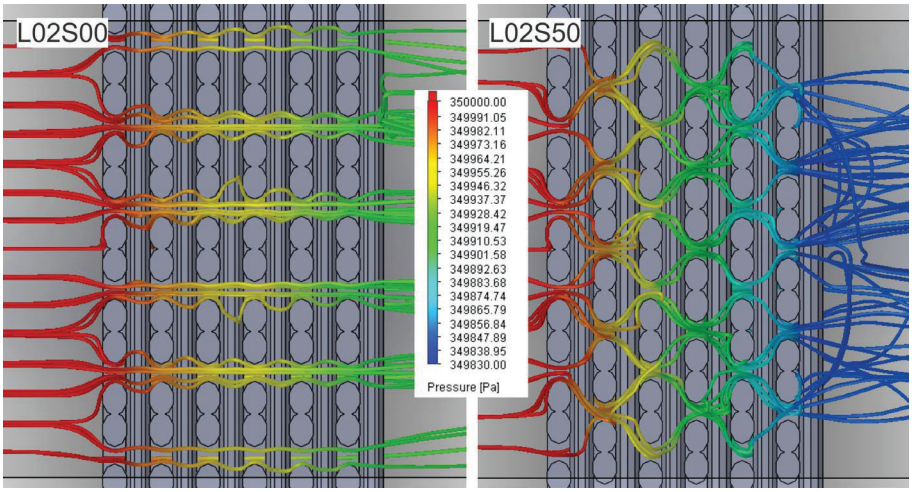

Fig. 8 – Cross section of L02S00 and L02S50 3D models with streamlines representing the pressure gradient

It is possible to observe that the permeability results, with the specific airflow conditions used, did not follow the same variation pattern. As the stagger distance increases from 0 to 50%, the decrease in permeability was more sensitive for the geometries with 2 filaments. In other words, these combinations presented a greater effect in the final permeability. Therefore, for a porous matrix with constant porosity, the increase in the stagger distance increases tortuosity, thus increasing the restriction imposed on the flow (the main hypothesis of this work). In general, a wider range in permeability, when varying the filling strategies, is positive because it allows accomplishing a wider range of applications.

Conclusions

The material extrusion AM with polymeric materials is an alternative to manufacturing PM with planned inner architecture and to achieve this better, it is necessary to have a process planning software with a high degree of customization of the filling parameters, eliminating the need to model the 3D pores.

In this study, two variants of the raster filling strategies were studied, one changing the stagger distance between layers and the other involving a new joined filaments proposal. Six PM designs were printed, and their permeabilities were measured experimentally and estimated numerically. The results indicate that both filling strategies influence the PM permeability, but the influence was more evident when the two parameters were combined (i.e., the number of joined filaments with the stagger distance). Especially for the case of 2 lines in set, it was observed that, as the stagger distance increases, the PM permeability decreases (i.e., a greater pressure drop), indicating that it is more difficult to pass the fluid through it.

Acknowledgements

To Repsol Sinopec Brasil S.A. for supporting the development of this research carried out according to ANP's research, development and innovation incentive law (No. 9478, 08/08/1997).

References

[1] P. Liu and G.-F. Chen, *Porous materials processing and applications*, 1st ed. Waltham, MA: Butterworth-Heinemann, 2014.

[2] M. G. M. Marascio, J. Antons, D. P. Pioletti, and P. E. Bourban, “3D Printing of Polymers with Hierarchical Continuous Porosity,” *Adv. Mater. Technol.*, vol. 2, no. 11, pp. 1–7, 2017.

[3] S. Ishutov *et al.*, “Three-dimensional printing for geoscience: Fundamental research, education, and applications for the petroleum industry,” *Am. Assoc. Pet. Geol. Bull.*, vol. 102, no. 1, pp. 1–26, Jan. 2018.

[4] N. Michailidis, A. Tsouknidas, L. Lefebvre, T. Hipke, and N. Kanetake, “Production, Characterization, and Applications of Porous Materials,” *Adv. Mater. Sci. Eng.*, vol. 2014, pp. 1–2, 2014.

[5] S. J. Kalita, S. Bose, H. L. Hosick, and A. Bandyopadhyay, “Development of controlled porosity polymer-ceramic composite scaffolds via fused deposition modeling,” *Mater. Sci. Eng. C*, vol. 23, no. 5, pp. 611–620, Oct. 2003.

[6] M. H. Too, K. F. Leong, C. K. Chua, C. M. Cheah, and S. L. Ho, “Feasibility of tissue engineering scaffold fabrication using fused deposition modelling,” in *The Seventh Australian and New Zealand Intelligent Information Systems Conference, 2001*, 2001, pp.

433–438.
[7] I. Zein, D. W. Hutmacher, K. C. Tan, and S. H. Teoh, “Fused deposition modeling of novel scaffold architectures for tissue engineering applications,” *Biomaterials*, vol. 23, no. 4, pp. 1169–1185, Feb. 2002.
[8] K. Chin Ang, K. Fai Leong, C. Kai Chua, and M. Chandrasekaran, “Investigation of the mechanical properties and porosity relationships in fused deposition modelling-fabricated porous structures,” *Rapid Prototyp. J.*, vol. 12, no. 2, pp. 100–105, Mar. 2006.
[9] L. Moroni, J. R. De Wijn, and C. A. Van Blitterswijk, “3D fiber-deposited scaffolds for tissue engineering: Influence of pores geometry and architecture on dynamic mechanical properties,” *Biomaterials*, vol. 27, no. 7, pp. 974–985, 2006.
[10] A. D. Olubamiji, Z. Izadifar, J. L. Si, D. M. L. Cooper, B. F. Eames, and D. X. Chen, “Modulating mechanical behaviour of 3D-printed cartilage-mimetic PCL scaffolds: influence of molecular weight and pore geometry,” *Biofabrication*, vol. 8, no. 2, p. 025020, Jun. 2016.
[11] J. M. Sobral, S. G. Caridade, R. A. Sousa, J. F. Mano, and R. L. Reis, “Three-dimensional plotted scaffolds with controlled pore size gradients: Effect of scaffold geometry on mechanical performance and cell seeding efficiency,” *Acta Biomater.*, vol. 7, no. 3, pp. 1009–1018, 2011.
[12] N. Volpato and J. A. Foggiatto, “The development of a generic Rapid Prototyping process planning system,” in *Innovative Developments in Design and Manufacturing - Advanced Research in Virtual and Rapid Prototyping*, 2009, pp. 381–387.
[13] L. Krambeck, G. A. Bartmeyer, D. Fusão, P. H. D. dos Santos, and T. A. Alves, “Permeability of a Capillary Structure of Sintered Copper Powder Used in Heat Pipes,” *Int. J. Adv. Eng. Res. Sci.*, vol. 6, no. 2, pp. 199–202, 2019.
[14] M. D. M. Innocentini, V. R. Salvini, A. Macedo, and V. C. Pandolfelli, “Prediction of ceramic foams permeability using Ergun’s equation,” *Mater. Res.*, vol. 2, no. 4, pp. 283–289, 2005.
[15] OpenSCAD, “OpenSCAD - The Programmers Solid 3D CAD Modeller,” 2019. [Online]. Available: http://http//www.openscad.org/. [Accessed: 26-Apr-2019].